CERN–TH/2000-073
hep-ph/0005233

Aspects of QCD, from the Tevatron to the LHC *†

Stefano Catani ‡

Theory Division, CERN, CH 1211 Geneva 23, Switzerland

Abstract

This contribution presents a selection of the topics (parton densities, fixed-order calculations, parton showers, soft-gluon resummation) discussed in my introductory lectures at the Workshop and includes a pedagogical overview of the corresponding theoretical tools.

CERN–TH/2000-073
February 2000

*To appear in the Proceedings of the Workshop *Physics at TeV Colliders*, Les Houches, France 8–18 June 1999.

†This work was supported in part by the EU Fourth Framework Programme "Training and Mobility of Researchers", Network "Quantum Chromodynamics and the Deep Structure of Elementary Particles", contract FMRX–CT98–0194 (DG 12 – MIHT).

‡On leave of absence from INFN, Sezione di Firenze, Florence, Italy.

1 Introduction

The production cross sections for all the processes at hadron-collider experiments are controlled by strong interaction physics and, hence, by its underlying field theory, QCD (see recent overviews in Refs. [1, 2, 3, 4]). Studies of QCD at the Tevatron and the LHC have two main purposes [5, 6, 7]. First, they are important to test the predictions of QCD, to measure its fundamental parameters (e.g. the strong coupling α_S) and to extract quantitative information on its non-perturbative dynamics (e.g. the distribution of partons in the proton). Second, they are relevant to a precise estimate of the background to other Standard Model processes and to signals of new physics.

This contribution is not a comprehensive review of QCD at high-energy hadron colliders. It is based on a selection of the topics presented in my introductory lectures at this Workshop. The selection highlights the QCD subjects that were most discussed during the Workshop and includes a pedagogical overview of some of the corresponding theoretical tools.

After the introduction of the general theoretical framework, I summarize in Sect. 2 the present knowledge on the parton densities and its impact on QCD predictions for hard-scattering processes at the Tevatron and the LHC. In Sect. 3, I then discuss some issues related to processes that are sensitive to the gluon density and, hence, to its determination. Section 4 presents a dictionary of different approaches (fixed-order expansions, resummed calculations, parton showers) to perturbative QCD calculations. The dictionary continues in Sect. 5, where I review soft-gluon resummation and discuss some recent phenomenological applications of threshold resummation to hadron collisions.

The QCD framework to describe any inclusive hard-scattering process,

$$h_1(p_1) + h_2(p_2) \to H(Q, \{\ldots\}) + X \quad , \tag{1}$$

in hadron–hadron collisions is based on perturbation theory and on the factorization theorem of mass singularities. The corresponding cross section is computed by using the factorization formula [8]

$$\begin{aligned}\sigma(p_1, p_2; Q, \{\ldots\}) = \sum_{a,b} \int_{x_{\min}}^{1} dx_1\, dx_2\, f_{a/h_1}(x_1, \mu_F^2)\, f_{b/h_2}(x_2, \mu_F^2)\, \hat{\sigma}_{ab}(x_1 p_1, x_2 p_2; Q, \{\ldots\}; \mu_F^2) \\ + \mathcal{O}\left((\Lambda_{QCD}/Q)^p\right) \quad .\end{aligned} \tag{2}$$

The colliding hadrons h_1 and h_2 have momenta p_1 and p_2, H denotes the triggered hard probe (vector bosons, jets, heavy quarks, Higgs bosons, SUSY particles and so on) and X stands for any unobserved particle produced by the collision. The typical scale Q of the scattering process is set by the invariant mass or the transverse momentum of the hard probe, and the notation $\{\ldots\}$ stands for any other relevant scale and kinematic variable of the process. For instance, in the case of W production we have $Q = M_W$ and $\{\ldots\} = \{Q_\perp, y, \ldots\}$, where $M_W, Q_\perp$ and y are the mass of the vector boson, its transverse momentum and its rapidity, respectively.

The factorization formula (2) involves the convolution of the partonic cross sections $\hat{\sigma}_{ab}$ (where $a, b = q, \bar{q}, g$) and the parton distributions $f_{a/h}(x, \mu_F^2)$ of the colliding hadrons. If

the hard probe H is a hadron or a photon, the factorization formula has to include an additional convolution with the corresponding parton fragmentation function $d_{a/H}(z, \mu_F^2)$.

The term $\mathcal{O}\left((\Lambda_{QCD}/Q)^p\right)$ on the right-hand side of Eq. (2) generically denotes non-perturbative contributions (hadronization effects, multiparton interactions, contributions of the soft underlying event, and so on). Provided the hard-scattering process (1) is sufficiently inclusive[§], $\hat{\sigma}_{ab}$ is computable as a power series expansion in $\alpha_{\mathrm{S}}(Q^2)$ and the non-perturbative contributions are (small) power-suppressed corrections (i.e. the power p is positive) as long as the hard-scattering scale Q is larger than few hundred MeV, the typical size of the QCD scale Λ_{QCD}.

The parton densities $f_{a/h}(x, \mu_F^2)$ are phenomenological distributions that describe how partons are bounded in the colliding hadrons. Although they are not calculable in QCD perturbation theory, the parton densities are universal (process-independent) quantities. The scale μ_F is a factorization scale introduced in Eq. (2) to separate the bound-state effects from the perturbative interactions of the partons. The physical cross section $\sigma(p_1, p_2; Q, \{\ldots\})$ does not depend on this arbitrary scale, but parton densities and partonic cross sections separately depend on μ_F. In particular, higher-order contributions to $\hat{\sigma}_{ab}(x_1 p_1, x_2 p_2; Q, \{\ldots\}; \mu_F^2)$ contain corrections of relative order $(\alpha_{\mathrm{S}}(Q^2) \ln Q^2/\mu_F^2)^n$. If μ_F is very different from Q, these corrections become large and spoil the reliability of the perturbative expansion. Thus, in practical applications of the factorization formula (2), the scale μ_F is set approximately equal to the hard scale Q and variations of μ_F around this central value are used to estimate the uncertainty of the perturbative expansion.

The lower limit $x_{\min}$ of the integrations over the parton momentum fractions x_1 and x_2, as well as the values of x_1 and x_2 that dominate the convolution integral in Eq. (2), are controlled by the kinematics of the hard-scattering process. Typically we have $x_{\min} \gtrsim Q^2/S$, where $S = (p_1 + p_2)^2$ is the square of the centre-of-mass energy of the collision. If the hard probe is a state of invariant mass M and rapidity y, the dominant values of the momentum fractions are $x_{1,2} \sim (M e^{\pm y})/\sqrt{S}$ (see Fig. 1). Thus varying M and y at fixed $\sqrt{S}$, we are sensitive to partons with different momentum fractions. Increasing $\sqrt{S}$ the parton densities are probed in a kinematic range that extends towards larger values of Q and smaller values of $x_{1,2}$.

2 Parton densities

The parton densities are an essential ingredient to study hard-scattering collisions. Once the partonic cross sections have been perturbatively computed, cross section measurements can be used to determine the parton densities. Then, they can in turn be used to predict cross sections for other hard-scattering processes.

The dependence of the parton densities[¶] $f_a(x, \mu^2)$ on the momentum fraction x and their absolute value at any fixed scale μ are not computable in perturbation theory. However,

[§] More precisely, it has to be defined in an infrared- and collinear-safe manner.

[¶] In the following the parton densities of the proton $f_{a/p}$ are simply denoted by f_a and those of the antiproton are obtained by using charge-conjugation invariance, i.e. $f_{a/\bar{p}} = f_{\bar{a}/p} = f_{\bar{a}}$.

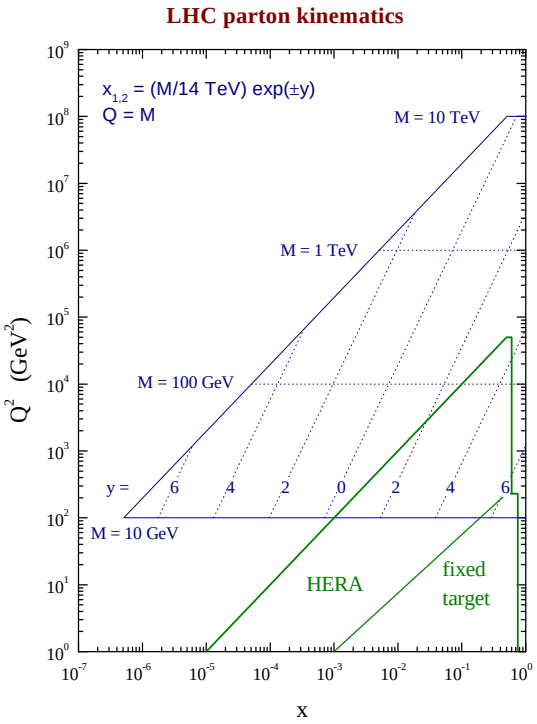

Figure 1: The (x, Q^2) plane of the parton kinematics for the production of a heavy system of invariant mass M and rapidity y at LHC, HERA and fixed-target experiments.

the scale dependence is perturbatively controlled by the DGLAP evolution equation [9]

$$\frac{d\, f_a(x,\mu^2)}{d \ln \mu^2} = \sum_b \int_x^1 \frac{dz}{z}\, P_{ab}(\alpha_{\rm S}(\mu^2), z)\, f_a(x/z, \mu^2) \quad . \tag{3}$$

The kernels $P_{ab}(\alpha_{\rm S}, z)$ are the Altarelli–Parisi (AP) splitting functions. As the partonic cross sections in Eq. (2), the AP splitting functions can be computed as a power series expansion in $\alpha_{\rm S}$:

$$P_{ab}(\alpha_{\rm S}, z) = \alpha_{\rm S} P_{ab}^{(LO)}(z) + \alpha_{\rm S}^2 P_{ab}^{(NLO)}(z) + \alpha_{\rm S}^3 P_{ab}^{(NNLO)}(z) + \mathcal{O}(\alpha_{\rm S}^4) \quad . \tag{4}$$

The leading order (LO) and next-to-leading order (NLO) terms $P_{ab}^{(LO)}(z)$ and $P_{ab}^{(NLO)}(z)$ in the expansion are known [10]. These first two terms are used in most of the QCD studies. Having determined $f_a(x, Q_0^2)$ at a given input scale $\mu = Q_0$, the evolution equation (3) can be used to compute the parton densities at different perturbative scales μ and larger values of x.

The parton densities are determined by performing global fits [11] to data from deep-inelastic scattering (DIS), Drell–Yan (DY), prompt-photon and jet production. The method consists in parametrizing the parton densities at some input scale Q_0 and then adjusting the parameters to fit the data. The parameters are usually constrained by imposing the positivity of the parton densities ($f_a(x, \mu^2) \geq 0$) and the momentum sum rule ($\sum_a \int_0^1 dx\, x\, f_a(x, \mu^2) = 1$).

The present knowledge on the parton densities of the proton is reviewed in Refs. [7, 12]. Their typical behaviour is shown in Fig. 2. All densities decrease at large x. At small x the valence quark densities vanish and the gluon density dominates. The sea-quark densities

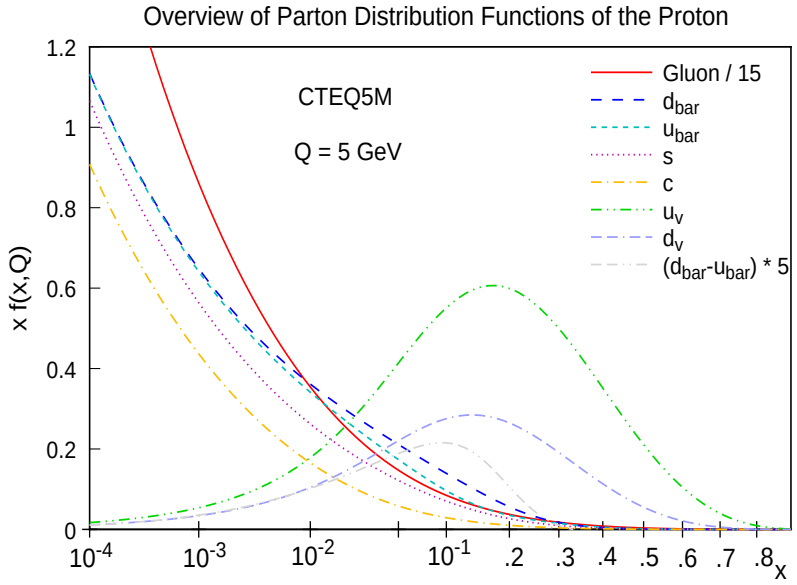

Figure 2: Typical x-shape of the parton densities (set CTEQ5M at $Q = 5$ GeV).

also increase at small x because they are driven by the strong rise of the gluon density and the splitting of gluons in $q\bar{q}$ pairs. Note that the quark densities are not flavour-symmetric either in the valence sector ($u_v \neq d_v$) or in the sea sector ($\bar{u} \neq \bar{d}$).

In addition to having the best estimate of the parton densities, it is important to quantify the corresponding uncertainty. This is a difficult issue. The uncertainty depends on the kinematic range in x and Q^2. Moreover, it cannot be reliably estimated by simply comparing the parton densities obtained by different global fits. In fact, a lot of common systematic and common assumptions affect the global-fit procedures. Recent attempts to obtain parton densities with error bands that take into account correlations between experimental errors are described in Refs. [7, 13]. Some important theoretical uncertainties that are still to be understood are also discussed in Ref. [7].

The overall conclusion is that the quark densities[‖] are reasonably well constrained and determined by DIS and DY processes, while the gluon density is certainly more uncertain [11, 17]. At small x ($x \lesssim 10^{-3}$), the gluon density f_g is at present constrained by a *single* process, namely DIS at HERA. Thus, large higher-order corrections of the type $(\alpha_S \ln 1/x)^n$ could possibly affect the extraction of f_g. *Assuming* that f_g is well determined at small x, the momentum sum rule reasonably constrains f_g at intermediate values of x ($x \sim 10^{-2}$). Jet production at the Tevatron at low to moderate values of the jet transverse energy E_T can also be useful in constraining the gluon distribution in the range $0.05 \lesssim x \lesssim 0.2$. At large x ($x \sim 10^{-1}$), the most sensitive process to f_g is prompt-photon production. Since, at present, prompt-photon data are not well described/predicted by perturbative QCD calculations, they cannot be used for a precise determination of f_g. Further discussion on these points is given in Sect. 3.

The conclusion that the gluon density is not well known can also be drawn by inspection (see Fig. 3) of the differences between the most updated analyses performed by the CTEQ

[‖]Uncertainties on the determination of the quark densities at very high x are discussed in Refs. [14, 15, 16].

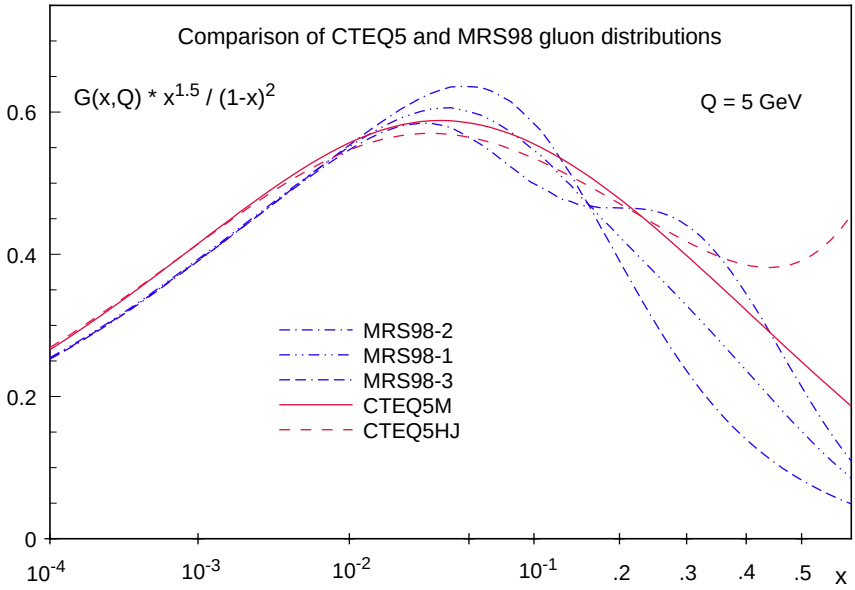

Figure 3: Comparison between the gluon densities of the CTEQ and MRST groups.

Collaboration and the MRST group.

The differences between the MRST gluons and the CTEQ ones are due to the fact that the two groups used different data sets. The various gluon densities are very similar at small x, because in this region both groups used the HERA data. The MRST group includes prompt-photon data in the global fit: these data constrain the gluon directly at $x \gtrsim 10^{-1}$ and indirectly (by the momentum sum rule) at $x \sim 10^{-2}$. The CTEQ group does not use prompt-photon data, but it includes Tevatron data on the one-jet inclusive cross section. These data give a good constraint on f_g in the region $10^{-2} < x < 10^{-1}$.

There are also differences within the MRST and CTEQ sets. The various gluon densities of the MRST set correspond to different values of the non-perturbative transverse-momentum smearing that can be introduced to describe the differences among the prompt-photon data that are available at several centre-of-mass energies. The CTEQ5M and CTEQ5HJ gluons correspond to different assumptions on the parametrization of the functional form of $f_g(x, Q_0^2)$ at large x; the CTEQ5M set corresponds to the minimum-χ^2 solution of the fit while the CTEQ5HJ set (with a slightly higher χ^2) provides the best fit to the high-E_T tail of the CDF *and* D0 jet cross sections.

This brief illustration shows that the differences in the most recent parton densities are mainly due to either inconsistencies between data sets and/or poor theoretical understanding of them. A more quantitative picture of the dependence on x and Q^2 of the gluon density uncertainty is presented in Fig. 4.

We can see that the DIS and DY data sets weakly constrain f_g for $x \gtrsim 10^{-1}$. Since the AP splitting functions lead to negative scaling violation at large x, when $f_g(x, Q^2)$ is evolved at larger scales Q according to Eq. (3) the gluon uncertainty is diluted: it propagates at smaller values of x and its size is reduced at fixed x.

Figure 5 shows the typical predictions for hard-scattering cross sections at the Tevatron and the LHC, as obtained by using the parton densities of the MRST set. These predic-

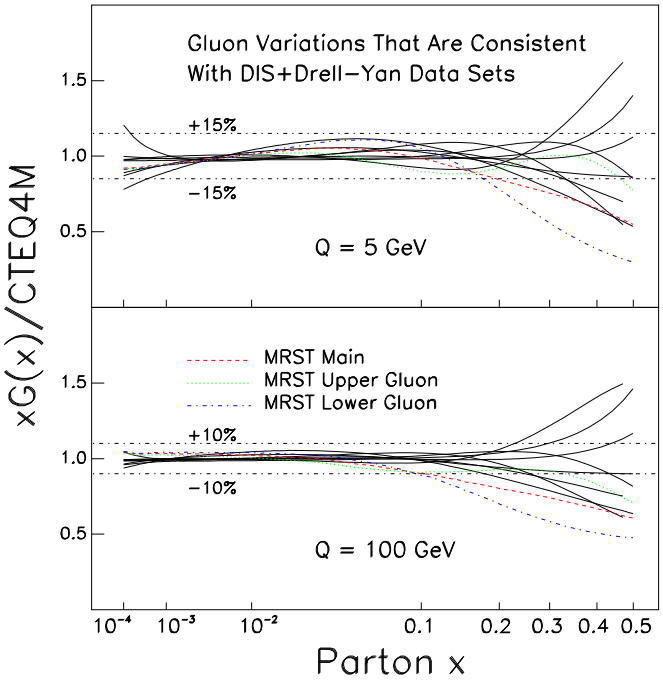

Figure 4: A picture of the gluon density uncertainty. The continuous (black) lines refer to gluon densities that are constrained only by DIS and DY data. The dashed (coloured) lines refer to gluon densities of the MRST group, which uses also prompt-photon data.

tions have to be supplemented with the corresponding uncertainties [7] coming from the determination of the parton densities and from perturbative corrections beyond the NLO. Owing to the increased centre-of-mass energy and to QCD scaling violation (see Fig. 4), the kinematic region with small uncertainties is larger at the LHC than at the Tevatron.

For most of the QCD processes at the LHC, the uncertainty from the parton densities is smaller than $\pm 10\%$ and, in particular, it is smaller than the uncertainty from higher-order corrections. Some relevant exceptions are the single-jet, W/Z and top quark cross sections. In the case of the single-jet inclusive cross section at high E_T ($E_T \gtrsim 2$ TeV), the uncertainty from the poorly known gluon density at high x is larger than that ($\sim \pm 10\%$) from higher-order corrections. The W and Z production cross sections are dominated by $q\bar{q}$ annihilation. Since the quark densities are well known, the ensuing uncertainty on the W/Z cross section is small ($\sim \pm 5\%$). Nonetheless, in this case the uncertainty from higher-order corrections is even smaller, since the partonic cross sections for the DY process are known [18] at the next-to-next-to-leading order (NNLO) in perturbation theory. In the case of top-quark production at the LHC, the gluon channel dominates and leads to an uncertainty of $\pm 10\%$ on the total cross section. Also for this process, however, the perturbative component is known beyond the NLO. Including all-order resummation of soft-gluon contributions [19], the estimated uncertainty from unknown higher-order corrections is approximately $\pm 5\%$ [19, 7].

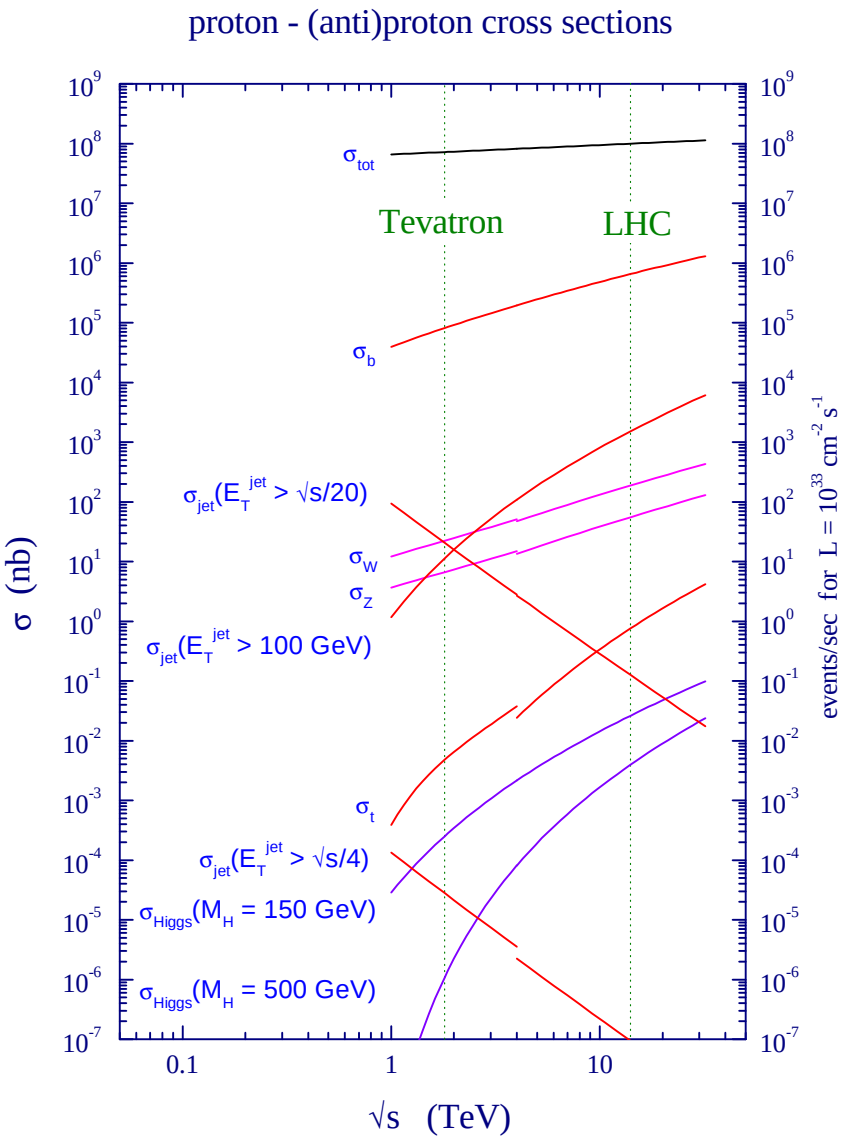

Figure 5: QCD predictions for hard-scattering cross sections at the Tevatron and the LHC.

3 The gluon density issue

At present, the processes** that are, in principle, most sensitive to the gluon density are DIS at HERA, b-quark production at the Tevatron, and prompt-photon production at fixed-target experiments. These processes constrain f_g for $x \lesssim 10^{-3}$, $x \sim 10^{-3}$–10^{-2} and $x \gtrsim 10^{-1}$, respectively. Nonetheless, the gluon density is, in practice, not well determined. The issue (or, perhaps, the puzzle) is that from a phenomenological viewpoint the standard theory, namely perturbative QCD at NLO, works pretty well for $x \lesssim 10^{-3}$ but not so well at larger values of x, while from theoretical arguments we should expect just the opposite to happen. This issue is discussed below mainly in its perturbative aspects. We should however keep it in mind that all these processes are dominated by hard-scattering scales Q of the order of few GeV. Different types of non-perturbative contributions can thus be important.

From the study of DIS at HERA we can extract information on the gluon and sea-quark densities of the proton. The main steps in the QCD analysis of the structure functions at small values of the Bjorken variable x are the following. The measurement of the proton structure function $F_2(x,Q^2) \sim q_S(x,Q^2)$ directly determines the sea-quark density $q_S = x(f_q + f_{\bar{q}})$. Then, the DGLAP evolution equation (3) or, more precisely, the following equations (the symbol $\otimes$ denotes the convolution integral with respect to x):

$$dF_2(x,Q^2)/d\ln Q^2 \;\sim\; P_{qq} \otimes q_S + P_{qg} \otimes g \;\;, \tag{5}$$

$$dg(x,Q^2)/d\ln Q^2 \;\sim\; P_{gq} \otimes q_S + P_{gg} \otimes g \;\;, \tag{6}$$

are used to extract a gluon density $g(x,Q^2) = xf_g(x,Q^2)$ that agrees with the measured scaling violation in $dF_2(x,Q^2)/d\ln Q^2$ (according to Eq. (5)) and fulfils the self-consistency equation (6).

The perturbative-QCD ingredients in this analysis are the AP splitting functions $P_{ab}(\alpha_S, x)$. Once they are known (and only then), the non-perturbative gluon density can be determined.

The standard perturbative-QCD framework to extract $g(x,Q^2)$ consists in using the truncation of the AP splitting functions at the NLO. This approach has been extensively compared with structure function data over the last few years and it gives a good description of the HERA data, down to low values of $Q^2 \sim 2\,\mathrm{GeV}^2$. The NLO QCD fits simply require a slightly steep input gluon density at these low momentum scales. Typically [11], we have $g(x,Q_0^2) \sim x^{-\lambda}$, with $\lambda \sim 0.2$ at $Q_0^2 \sim 2\,\mathrm{GeV}^2$, and the data constrain $g(x,Q_0^2)$ with an uncertainty of approximately $\pm 20\%$.

Although it is phenomenologically successful, the NLO approach is not fully satisfactory from a theoretical viewpoint. The truncation of the splitting functions at a fixed perturbative order is equivalent to assuming that the dominant dynamical mechanism leading to scaling violations is the evolution of parton cascades with strongly-ordered transverse momenta. However, at high energy this evolution takes place over large rapidity intervals ($\Delta y \sim \ln 1/x$) and diffusion in transverse momentum becomes relevant. Formally, this

**The rôle of jet production at the Tevatron has briefly been recalled in Sect. 2, and it is discussed in detail in Ref. [12].

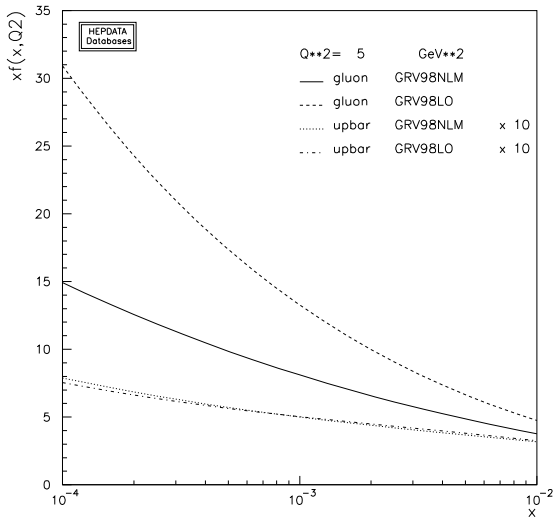

Figure 6: Comparison between the LO (GRV98LO) and NLO (GRV98NLM) GRV parametrizations of the gluon and sea-quark densities at $Q^2 = 5$ GeV^2.

implies that higher-order corrections to $P_{ab}(\alpha_S, x)$ are logarithmically enhanced:

$$P_{ab}(\alpha_S, x) \sim \frac{\alpha_S}{x} + \frac{\alpha_S}{x}\,(\alpha_S \ln x) + \ldots + \frac{\alpha_S}{x}\,(\alpha_S \ln x)^n + \ldots \quad . \tag{7}$$

At asymptotically small values of x, resummation of these corrections is mandatory to obtain reliable predictions.

Small-x resummation is, in general, accomplished by the BFKL equation [20]. In the context of structure-function calculations, the BFKL equation provides us with improved expressions of the AP splitting functions $P_{ab}(\alpha_S, x)$, in which the leading logarithmic (LL) terms $(\alpha_S \ln x)^n$, the next-to-leading logarithmic (NLL) terms $\alpha_S(\alpha_S \ln x)^n$, and so forth, are systematically summed to all orders n in α_S. The present theoretical status of small-x resummation is discussed in Ref. [7]. Since in the small-x region the gluon channel dominates, only the gluon splitting functions P_{gg} and P_{gq} contain LL contributions. These are known [20, 21] to be positive but numerically smaller than naively expected (the approach to the asymptotic regime is much delayed by cancellations of logarithmic corrections that occur at the first perturbative orders in P_{gg} and P_{gq}). The NLL terms in the quark splitting functions P_{qg} and P_{qq} are known [22] and turn out to be positive and large. A very important progress is the recent calculation [23, 24] of the NLL terms in P_{gg}, which are found to be negative and large. The complete NLL terms in P_{gq} are still unknown.

The results of Refs. [23, 24], the large size of the NLL terms and the alternating sign (from the LL to the NLL order and from the gluon to the quark channel) of the resummed small-x contributions have prompted a lot of activity (see the list of references in Ref. [7]) on the conceptual basis and the phenomenological implications of small-x resummation. This activity is still in progress and definite quantitative conclusions on the impact of small-x resummation at HERA cannot be drawn yet.

At the same time, the capability of the fixed-order approach to produce a good description of the proton structure function $F_2(x, Q^2)$ at HERA cannot be used to conclude that the small-x behaviour of the gluon density is certainly well determined. In fact, by

comparing LO and NLO results, we could argue that the ensuing theoretical uncertainty on f_g is sizeable [4]. Going from LO to NLO, we can obtain stable predictions for F_2, but we have to vary the gluon density a lot. As shown in Fig. 6, the NLO gluon density sizeably differs from its LO parametrization, not only in absolute normalization but also in x-shape. For instance, at $x = 10^{-4}$ and $Q^2 = 5$ GeV^2 the NLO gluon is a factor of 2 smaller than the LO gluon. This can be understood [25] from the fact that the scaling violation of F_2 is produced by the convolution $P_{qg} \otimes g$ (see the right-hand side of Eq. (5)). The quark splitting function P_{qg} behaves as

$$P_{qg}(\alpha_{\rm S}, x) \simeq \alpha_{\rm S} P_{qg}^{(LO)}(x) \left[1 + 2.2 \frac{C_A \alpha_{\rm S}}{\pi} \frac{1}{x} + \ldots\right] \quad , \tag{8}$$

where the LO term $P_{qg}^{(LO)}(x)$ is flat at small x, whereas the NLO correction is steep. To obtain a stable evolution of F_2, the NLO steepness of P_{qg} has to be compensated by a gluon density that is less steep at NLO than at LO. This has to be kept in mind when concluding on the importance of small-x resummation because the NLO steepness of P_{qg} is the lowest-order manifestation of BFKL dynamics in the quark channel.

In the large-x region, there is a well-known correlation between $\alpha_{\rm S}$ and f_g. At small x, there is an analogous strong correlation between the x-shapes of P_{qg} and f_g. In the fixed-order QCD analysis of F_2, large NLO perturbative corrections at small x can be balanced by the extreme flexibility of parton density parametrizations. It is difficult to disentangle this correlation between process-dependent perturbative contributions and non-perturbative parton densities from the study of a single quantity, as in the case of F_2 at HERA. The uncertainty on the gluon density at small x, as estimated from the NLO QCD fits of the HERA data, is evidently only a lower limit on the actual uncertainty on f_g.

The production of b quarks at the Tevatron is also sensitive to the gluon density at relatively small values of x. The comparison between Tevatron data and perturbative-QCD predictions at NLO [26] is shown in Fig. 7. Using standard sets of parton densities, the theoretical predictions typically underestimate the measured cross section by a factor of 2. This certainly is disappointing, although justifiable by the large theoretical uncertainty of the perturbative calculation [28]. A lower limit on this uncertainty can be estimated by studying the scale dependence and the convergence of the perturbative expansion. Varying the factorization and renormalization scales by a factor of four around the b-quark mass m_b, the NLO cross section varies by a factor of almost 2 at the Tevatron and by a factor of 4–5 at the LHC [7]. Similar factors are obtained by considering the ratio of the NLO and LO cross sections.

The present theoretical predictions for b-quark production at hadron colliders certainly need to be improved [7]. Since the hard scale $Q \sim m_b$ is not very large, a possible improvement regards estimates of non-perturbative contributions (for instance, effects of the fragmentation of the b-quark and of the intrinsic transverse momentum of the colliding partons). As for the evaluation of perturbative contributions at higher orders, the resummation of logarithmic terms of the type $\alpha_{\rm S}^n \ln^n(p_t/m_b)$ is important [29] when the transverse momentum p_t of the b quark is much larger than m_b. The resummation of small-x logarithmic contributions $\alpha_{\rm S}^n \ln^n x$ can also be relevant, because $x \sim 2m_b/\sqrt{S}$ is as small as $\sim 10^{-3}$ at the Tevatron and as $\sim 10^{-4}$ at the LHC. The theoretical tool to perform this resummation, namely the $k_\perp$-factorization approach [30], is available. Updated phenomenological

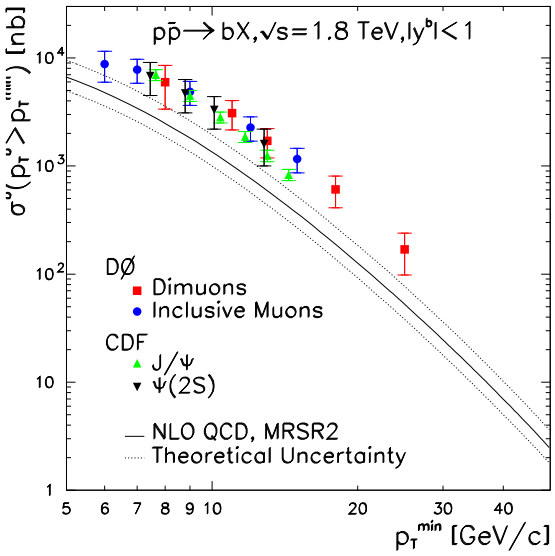

Figure 7: Comparison between Tevatron data and NLO QCD for b-quark production [27]. The band is obtained by varying factorization and renormalization scales in the NLO calculation.

studies based on this tool and on the information from small-x DIS at HERA would be interesting.

Prompt-photon production at fixed-target experiments is sensitive to the behaviour of the gluon density at large x ($x \gtrsim 0.1$). The theoretical predictions for this process, however, are not very accurate. Figure 8 shows the factorization- and renormalization-scale dependence of the perturbative cross section for the case of the E706 kinematics. If the scale is varied by a factor of 4 around the transverse energy E_T of the prompt photon, the LO cross section varies by a factor of almost 4. Going to NLO [31] the situation improves, but not very much, because the NLO cross section still varies by a factor of about 2.

A detailed comparison between NLO QCD calculations and data from the ISR and fixed-target experiments has recently been performed in Ref. [32]. As shown in Fig. 9, the overall agreement with the theory is not satisfactory, even taking into account the uncertainty coming from scale variations in the theoretical predictions. Modifications of the gluon density can improve the agreement with some data sets only at the expense of having larger disagreement with other data sets. The differences between experiments at similar centre-of-mass energies (see, for instance, E706 pBe/530 at $\sqrt{S} = 31.6$ GeV and WA70 pp at $\sqrt{S} = 23$ GeV) are much larger than expected from perturbative scaling violations. This can possibly suggest [32] inconsistencies of experimental origin.

Another (not necessarily alternative) origin of the differences between data and theory could be the presence of non-perturbative effects that are not included in the NLO perturbative calculation. This explanation has been put forward in Refs. [33, 34] by introducing some amount of intrinsic[††] transverse momentum $\langle k_\perp \rangle$ of the colliding partons.

[††]To be precise, in Ref. [34] the $\langle k_\perp \rangle$ of the colliding partons is not called 'intrinsic', but it is more

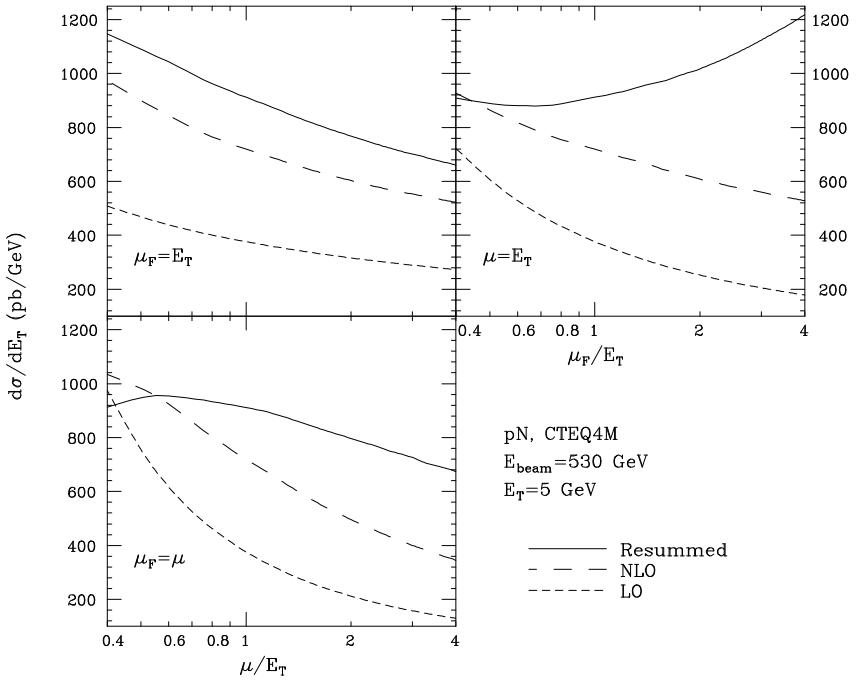

Figure 8: The dependence on the factorization (μ_F) and renormalization ($\mu_R = \mu$) scale of the LO and NLO prompt-photon cross section $d\sigma/dE_T$ in pN collisions at $E_T = 5$ GeV and $\sqrt{S} = 31.6$ GeV. The resummed calculation is discussed in Sect. 5.

Owing to the steeply falling E_T distribution ($d\sigma/dE_T \propto 1/E_T^7$) of the prompt photon, even a small transverse-momentum kick[‡‡] can indeed produce a large effect on the cross section, in particular, at small values of E_T. Phenomenological investigations [34] show that this additional $\langle k_\perp \rangle$ kick can lead to a better agreement between calculations and data. The E706 data suggest the value $\langle k_\perp \rangle \sim 1.2$ GeV, the WA70 data prefer no $\langle k_\perp \rangle$, and the UA6 data in the intermediate range of centre-of-mass energy ($\sqrt{S} = 24.3$ GeV) may prefer an intermediate value of $\langle k_\perp \rangle$. Similar conclusions are obtained in the analysis by the MRST group [11].

A precise physical understanding of $\langle k_\perp \rangle$ effects is still missing. On one side, since the amount of $\langle k_\perp \rangle$ suggested by prompt-photon data varies with $\sqrt{S}$, it is difficult to argue that the transverse momentum is really 'intrinsic' and has an entirely non-perturbative origin. On the other side, in the case of the inclusive production of a single photon, a similar effect cannot be justified by higher-order *logarithmic* corrections produced by perturbative soft-gluon radiation (see Sect. 5). A lot of model-dependent assumptions (and ensuing uncertainties) certainly enter in the present implementations of the $\langle k_\perp \rangle$ kick. A general framework to *consistently* include non-perturbative transverse-momentum effects in perturbative calculations is not yet available. Recent proposals with this aim are presented in Refs. [35] and [36].

Further studies on the consistency between different prompt-photon experiments and

generically called the $\langle k_\perp \rangle$ 'from initial-state soft-gluon radiation'.

[‡‡]The E_T distribution of the single-photon is not calculable down to $E_T = 0$ or, in other words, $d\sigma/dE_T$ is not integrable in the entire kinematic range of E_T. Thus, the intrinsic $\langle k_\perp \rangle$ of the incoming partons does not simply produce a shift of events from the low-E_T to the high-E_T region. For this reason, the terminology '$\langle k_\perp \rangle$ kick' seems to be more appropriate than '$\langle k_\perp \rangle$ smearing'.

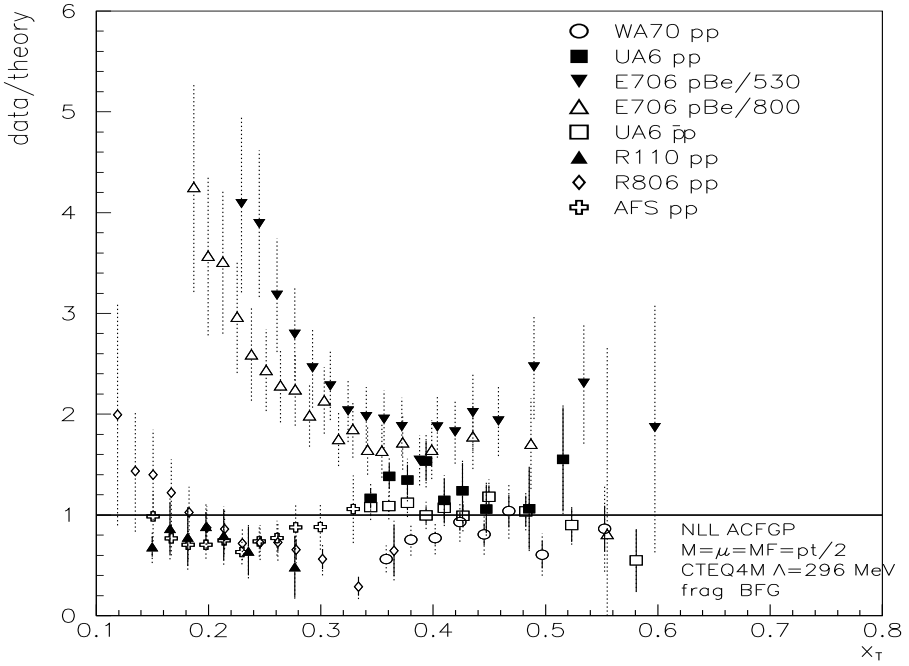

Figure 9: A comparison between NLO QCD calculations and data from the ISR and fixed-target experiments for the prompt-photon distribution $d\sigma/dE_T$ ($x_T = 2E_T/\sqrt{S}$).

on the issue of intrinsic-$\langle k_\perp \rangle$ effects in hadron–hadron collisions are necessary. Owing to the present theoretical (and, possibly, experimental) uncertainties, it is difficult to use prompt-photon data to accurately determine the gluon density at large x. Other recent theoretical improvements, such as soft-gluon resummation, of the perturbative calculations for prompt-photon production at large $x_T = 2E_T/\sqrt{S}$ are discussed in Sect. 5.

Studies of other single-particle inclusive cross sections, such as π^0 cross sections [34, 37, 38], can be valuable to constrain the parton densities and could possibly help to clarify some of the experimental and theoretical issues arisen by prompt-photon production.

4 Partonic cross sections: fixed-order expansions, resummed calculations, parton showers

The calculation of hard-scattering cross sections according to the factorization formula (2) requires the knowledge of the partonic cross sections $\hat{\sigma}$, besides that of the parton densities. The partonic cross sections are usually computed by truncating their perturbative expansion at a fixed order in $\alpha_{\rm S}$:

$$\begin{aligned}\hat{\sigma}(p_1,p_2;Q,\{Q_1,\ldots\};\mu_F^2) = \alpha_{\rm S}^k(\mu_R^2)\,\Big\{&\hat{\sigma}^{(LO)}(p_1,p_2;Q,\{Q_1,\ldots\}) \\ &+\alpha_{\rm S}(\mu_R^2)\;\hat{\sigma}^{(NLO)}(p_1,p_2;Q,\{Q_1,\ldots\};\mu_R^2;\mu_F^2) \\ &+\alpha_{\rm S}^2(\mu_R^2)\;\hat{\sigma}^{(NNLO)}(p_1,p_2;Q,\{Q_1,\ldots\};\mu_R^2;\mu_F^2)+\ldots\Big\}\,.\end{aligned} \tag{9}$$

The scale μ_R is the arbitrary renormalization scale introduced to define the perturbative expansion. Although the 'exact' partonic cross section on the left-hand side of Eq. (9)

does not depend on μ_R, each term on the right-hand side (and, hence, any fixed-order truncation) separately depends on it.

The LO (or tree-level) term $\hat{\sigma}^{(LO)}$ gives only an estimate of the order of magnitude of the partonic cross section, because at this order α_S is not unambiguously defined. Equivalently, we can say that since $\hat{\sigma}^{(LO)}$ does not depend on μ_R, the size of its contribution can be varied quite arbitrarily by changing μ_R in its coefficient $\alpha_S^k(\mu_R^2)$. The strong coupling α_S can be precisely defined only starting from NLO. A 'reliable' estimate of the central value of $\hat{\sigma}$ thus requires the knowledge of (at least) the NLO term $\hat{\sigma}^{(NLO)}$. This term explicitly depends on μ_R and this dependence begins to compensate that of $\alpha_S(\mu_R^2)$.

In general, the n-th term in the curly bracket of Eq. (9) contains contributions of the type $(\alpha_S(\mu_R^2)\ln Q/\mu_R)^n$. If μ_R is very different from the hard scale Q, these contributions become large and spoil the reliability of the truncated expansion (9). Thus, in practical applications the scale μ_R should be set approximately equal to the hard scale Q. As mentioned in Sect. 3, variations of μ_R around this central value are typically used to set a lower limit on the theoretical uncertainty of the perturbative calculation.

A better estimate of the accuracy of any perturbative expansion is obtained by considering the effect of removing the last perturbative term that has been computed. Since α_S can be precisely defined only at NLO, this procedure can consistently be applied to Eq. (9) only as from its NNLO term. A 'reliable' estimate of the theoretical error on $\hat{\sigma}$ thus requires the knowledge of the NNLO term $\hat{\sigma}^{(NNLO)}$ in Eq. (9).

The LO and NLO approximations of $\hat{\sigma}$ are used at present in (most of) the fixed-order QCD calculations. Prospects towards NNLO calculations of partonic cross sections and AP splitting functions are reviewed in Refs. [7, 39].

The fixed-order expansion (9) provides us with a well-defined and systematic framework to compute the partonic cross section $\hat{\sigma}(p_1, p_2; Q, \{Q_1, \ldots\}; \mu_F^2)$ of any hard-scattering process that is sufficiently inclusive or, more precisely, that is defined in an infrared- and collinear-safe manner. However, the fixed-order expansion is reliable only when all the kinematical scales $Q, \{Q_1, \ldots\}$ are of the same order of magnitude. When the hard-scattering process involves two (or several) very different scales, say $Q_1 \gg Q$, the $\mathrm{N}^n\mathrm{LO}$ term in Eq. (9) can contain double- and single-logarithmic contributions of the type $(\alpha_S L^2)^n$ and $(\alpha_S L)^n$ with $L = \ln(Q_1/Q) \gg 1$. These terms spoil the reliability of the fixed-order expansion and have to be summed to all orders by systematically defining logarithmic expansions (resummed calculations).

Typical large logarithms, $L = \ln Q/Q_0$, are those related to the evolution of the parton densities from a low input scale Q_0 to the hard-scattering scale Q. These logarithms are produced by collinear radiation from the colliding partons and give single-logarithmic contributions. They never explicitly appear in the calculation of the partonic cross section, because they are systematically (LO, NLO and so forth) resummed in the evolved parton densities $f(x, Q^2)$ by using the DGLAP equation (3).

Different large logarithms, $L = \ln Q/\sqrt{S}$, appear when the centre-of-mass energy $\sqrt{S}$ of the collision is much larger than the hard scale Q. These small-x ($x = Q/\sqrt{S}$) logarithms are produced by multiple radiation over the wide rapidity range that is available at large

energy. They usually give single-logarithmic contributions that can be resummed by using the BFKL equation. BFKL resummation is relevant to DIS structure functions at small values of the Bjorken variable x (see Sect. 3) and it can also be important at the LHC for the production of b quarks and of prompt photons at relatively low E_T.

Another class of large logarithms is associated to the bremsstrahlung spectrum of soft gluons. Since soft gluons can be radiated collinearly, they give rise to double-logarithmic contributions to the partonic cross section:

$$\hat{\sigma} \sim \alpha_{\rm S}^k \hat{\sigma}^{(LO)} \left\{ 1 + \sum_{n=1}^{\infty} \alpha_{\rm S}^n \left(C_{2n}^{(n)} L^{2n} + C_{2n-1}^{(n)} L^{2n-1} + C_{2n-2}^{(n)} L^{2n-2} + \ldots \right) \right\} \quad . \tag{10}$$

Soft-gluon resummation is discussed in Sect. 5.

A related approach to evaluate higher-order contributions to the partonic cross sections is based on Monte Carlo parton showers (see [40] and the updated list of references in [6, 7]). Rather than computing exactly $\hat{\sigma}^{(NLO)}$, $\hat{\sigma}^{(NNLO)}$ and so forth, the parton shower gives an all-order approximation of the partonic cross section in the soft and collinear regions. In this respect, the computation of the partonic cross sections performed by parton showers is somehow similar to that obtained by soft-gluon resummed calculations. There is, however, an important conceptual difference between the two approaches. This difference and the limits of applicability of the parton-shower method are briefly recalled below. Apart from these limits, parton-shower calculations can give some advantages. Multiparton kinematics can be treated exactly. The parton shower can be supplemented with models of non-perturbative effects (hadronization, intrinsic $k_\perp$, soft underlying event) to provide a complete description of the hard-scattering process at the hadron level.

For a given cross section, resummed calculations can in principle be performed to any logarithmic accuracy. The logarithmic accuracy achievable by parton showers is instead intrinsically limited by quantum mechanics. The parton-shower algorithms are probabilistic. Starting from the LO cross section, the parton shower generates multiparton final states according to a probability distribution that approximates the *square* of the QCD matrix elements. The approximation is based on the universal (process-independent) factorization properties of multiparton matrix elements in the soft and collinear limits. Although the matrix element does factorize, its square contains quantum interferences, which are not positive-definite and, in general, cannot be used to define probability distributions. To leading infrared accuracy, this problem is overcome by exploiting QCD coherence (see Refs. [40, 41, 42] and referencees therein): soft gluons radiated at large angle from the partons involved in the LO subprocess destructively interfere. This quantum mechanical effect can be simply implemented by enforcing an angular-ordering constraint on the phase space available for the parton shower evolution. Thus, angular-ordered parton showers can *consistently* compute the first two dominant towers ($\alpha_{\rm S}^n L^{2n}$ and $\alpha_{\rm S}^n L^{2n-1}$) of logarithmic contributions in Eq. (10). However, parton showers contain also some subleading logarithmic contributions. For instance, they correctly compute the single-logarithmic terms $\alpha_{\rm S}^n L^n$ of purely collinear origin that lead to the LO evolution of the parton densities. Moreover, as discussed in Ref. [43] by a comparison with resummed calculations, in the case of hard-scattering processes whose LO subprocess involves two coloured partons (e.g. DIS or DY production), angular-ordered parton showers have a higher logarithmic accuracy: they can consistently evaluate the LL and NLL terms in Eq. (15). The extension of parton-shower

algorithms to higher logarithmic accuracy is not necessarily feasible and is, in any case, challenging.

Of course, because of quantum interferences and quantum fluctuations, the probabilistic parton-shower approach cannot be used to systematically perform exact calculations at NLO, NNLO and so forth. Nonetheless, important progress has been made to include matrix element corrections in parton shower algorithms [44–47]. The purpose is to consider the multiparton configurations generated by parton showering from the LO matrix element and to correct them in the hard (non-soft and non-collinear) region by using the exact expressions of the higher-order matrix elements. Hard matrix element corrections to parton showers have been implemented for top quark decay [48] and for production of W, Z and DY lepton pairs [49, 50, 51]. The same techniques could be applied to other processes, as, for instance, production of Higgs boson [52] and vector-boson pairs [7].

Note also that, at present, angular-ordered parton showers cannot be considered as true 'next-to-leading' tools, even where their logarithmic accuracy is concerned. The consistent computation of the first two towers of logarithmic contributions in Eq. (10) is not sufficient for this purpose. For instance, to precisely introduce an NLO definition of $\alpha_{\rm S}$, we should control all the terms obtained by the replacement $\alpha_{\rm S} \to \alpha_{\rm S} + c\ \alpha_{\rm S}^2 + \mathcal{O}(\alpha_{\rm S}^3)$. When it is introduced in the towers of double-logarithmic terms $\alpha_{\rm S}^n L^{2n}$ of Eq. (10), this replacement leads to contributions of the type $\alpha_{\rm S}^{n+1} L^{2n} \sim \alpha_{\rm S}^n L^{2n-2}$. Since these contributions are not fully computable at present, the parameter $\alpha_{\rm S}$ used in the parton showers corresponds to a simple LO parametrization of QCD running coupling.

5 Soft-gluon resummation

Double-logarithmic contributions due to soft gluons arise in all the kinematic configurations where radiation of real and virtual partons is highly unbalanced (see Ref. [53] and referenes therein). For instance, this happens in the case of transverse-momentum distributions at low transverse momentum, in the case of hard-scattering production near threshold or when the structure of the final state is investigated with high resolution (internal jet structure, shape variables).

Soft-gluon resummation for jet shapes has been extensively studied and applied to hadronic final states produced by e^+e^- annihilation [1, 4, 54]. Applications to hadron–hadron collisions have just begun to appear [55] and have a large, yet uncovered, potential (from $\alpha_{\rm S}$ determinations to studies of non-perturbative dynamics).

Transverse-momentum logarithms, $L = \ln Q^2/\boldsymbol{Q}_\perp^2$, occur in the distribution of transverse momentum $\boldsymbol{Q}_\perp$ of systems with high mass Q ($Q \gg Q_\perp$) that are produced with a vanishing $\boldsymbol{Q}_\perp$ in the LO subprocess. Examples of such systems are DY lepton pairs, lepton pairs produced by W and Z decay, heavy quark–antiquark pairs, photon pairs and Higgs bosons. In these processes the LO transverse-momentum distribution is sharply peaked around $\boldsymbol{Q}_\perp = 0$ ($d\hat{\sigma}/d^2\boldsymbol{Q}_\perp \propto \delta^{(2)}(\boldsymbol{Q}_\perp)$). If the heavy system is produced with $\boldsymbol{Q}_\perp^2 \ll Q$, the emission of real radiation at higher orders is strongly suppressed and cannot balance the virtual contributions. The ensuing logarithms, $L = \ln Q^2/\boldsymbol{Q}_\perp^2$, diverge order by order

when $\boldsymbol{Q}_\perp \to 0$, but after all-order resummation they leads to a finite smearing of the LO distribution.

Threshold logarithms, $L = \ln(1-x)$, occur when the tagged final state produced by the hard scattering is forced to carry a very large fraction x ($x \to 1$) of the available centre-of-mass energy $\sqrt{S}$. Also in this case, the radiative tail of real emission is stronly suppressed at higher perturbative orders. Oustanding examples of hard processes near threshold are DIS at large x (here x is the Bjorken variable), production of DY lepton pairs with large invariant mass Q ($x = Q/\sqrt{S}$), production of heavy quark–antiquark pairs ($x = 2m_Q/\sqrt{S}$), production of single jets and single photons at large transverse energy E_T ($x = 2E_T/\sqrt{S}$).

To emphasize the difference between transverse-momentum logarithms and threshold logarithms generated by soft gluons, it can be instructive to consider prompt-photon production. In the case of production of a *photon pair** with invariant mass squared $Q^2 = (p_1^{(\gamma)} + p_2^{(\gamma)})^2$ and *total* transverse momentum $\boldsymbol{Q}_\perp = \boldsymbol{p}_{1\perp}^{(\gamma)} + \boldsymbol{p}_{2\perp}^{(\gamma)}$, transverse-momentum logarithms and threshold logarithms appear when $\boldsymbol{Q}_\perp^2 \ll Q^2$ and $\boldsymbol{Q}_\perp^2 \sim (S/4 - Q^2)$, respectively. However, in the case of production of a *single photon* with transverse energy (or, equivalently, transverse momentum) E_T, soft gluons can produce logarithms only in the threshold region $x_T = 2E_T/\sqrt{S} \to 1$. If the prompt photon has a transverse energy that is not close† to its threshold value, the emission of accompanying radiation is not kinematically suppressed and there are no soft logarithms analogous to those in the transverse-momentum distribution of a photon pair. In particular, there are no double-logarithmic contributions of the type $(\alpha_S \ln^2 E_T^2/S)^n$, and perturbative soft gluons are not distinguishable from perturbative hard gluons.

Studies of soft-gluon resummation for transverse-momentum distributions at low transverse momentum and for hard-scattering production near threshold started two decades ago [42, 56]. The physical bases for a systematic all-order summation of the soft-gluon contributions are dynamics and kinematics factorizations [53]. The first factorization follows from gauge invariance and unitarity: in the soft limit, multigluon amplitudes fulfil factorization formulae given in terms of universal (process-independent) soft contributions. The second factorization regards kinematics and strongly depends on the actual cross section to be evaluated. *If*, in the appropriate soft limit, the multiparton phase space for this cross section can be written in a factorized way, resummation is analytically feasible in form of *generalized exponentiation* of the universal soft contributions that appear in the factorization formulae of the QCD amplitudes.

Note that the phase space depends in a non-trivial way on multigluon configurations and, in general, is not factorizable in single-particle contributions‡. Moreover, even when phase-space factorization is achievable, it does not always occur in the space of the kinematic variables where the cross section is defined. Usually, it is necessary to introduce a conjugate space to overcome phase-space constraints. This is the case for transverse-momentum distributions and hard-scattering production near threshold. The relevant kine-

*The same discussion applies to the production of a DY lepton pair.

†Eventually, when $x_T \ll 1$, higher-order corrections are single-logarithmically enhanced. This small-x logarithms, $(\alpha_S \ln x_T)^n$, have to be taken into account by BFKL resummation.

‡In the case of jet cross sections, for instance, phase-space factorization depends on the detailed definition of jets and it can easily be violated [57]. Some jet algorithms, such as the $k_\perp$-algorithm [58, 59], have better factorization properties.

matical constraint for $\boldsymbol{Q}_\perp$-distributions is (two-dimensional) transverse-momentum conservation and it can be factorized by performing a Fourier transformation. Soft-gluon resummation for $\boldsymbol{Q}_\perp$-distributions is thus carried out in $\boldsymbol{b}$-space [60, 61], where the impact parameter $\boldsymbol{b}$ is the variable conjugate to $\boldsymbol{Q}_\perp$ via the Fourier transformation. Analogously, the relevant kinematical constraint for hard-scattering production near threshold is (one-dimensional) energy conservation and it can be factorized by working in N-moment space [62, 63], N being the variable conjugate to the threshold variable x (energy fraction) via a Mellin or Laplace transformation.

Using a short-hand notation, the general structure of the partonic cross section $\hat{\sigma}$ after summation of soft-gluon contributions is

$$\hat{\sigma} = \hat{\sigma}_{\rm res.} + \hat{\sigma}_{\rm rem.} \ . \tag{11}$$

The term $\hat{\sigma}_{\rm res.}$ embodies the all-order resummation, while the remainder $\hat{\sigma}_{\rm rem.}$ contains no large logarithmic contributions. The latter has the form

$$\hat{\sigma}_{\rm rem.} = \hat{\sigma}^{\rm (f.o.)} - \left[\, \hat{\sigma}_{\rm res.} \,\right]^{\rm (f.o.)} \quad , \tag{12}$$

and it is obtained from $\hat{\sigma}^{\rm (f.o.)}$, the truncation of the perturbative expansion for $\hat{\sigma}$ at a given fixed order (LO, NLO, ...), by subtracting the corresponding truncation $[\hat{\sigma}_{\rm res.}]^{\rm (f.o.)}$ of the resummed part. Thus, the expression on the right-hand side of Eq. (11) includes soft-gluon logarithms to all orders and it is *matched* to the exact (with no logarithmic approximation) fixed-order calculation. It represents an improved perturbative calculation that is everywhere as good as the fixed-order result, and much better in the kinematics regions where the soft-gluon logarithms become large ($\alpha_{\rm S} L \sim 1$). Eventually, when $\alpha_{\rm S} L \gtrsim 1$, the resummed perturbative contributions are of the same size as the non-perturbative contributions and the effect of the latter has to be implemented in the resummed calculation.

The resummed cross section has the following typical form:

$$\hat{\sigma}_{\rm res.} = \alpha_{\rm S}^k \int_{\rm inv.} \hat{\sigma}^{(LO)} \cdot C \cdot S \ , \tag{13}$$

where the integral $\int_{\rm inv.}$ denotes the inverse tranformation from the conjugate space where resummation is actually carried out. Methods to perform the inverse transformation are discussed in Refs. [64] and [65] for $Q_\perp$-resummation and threshold resummation, respectively. The C term has the perturbative expansion

$$C = 1 + C_1 \, \alpha_{\rm S} + C_2 \, \alpha_{\rm S}^2 + \dots \tag{14}$$

and contains all the constant contributions in the limit $L \to \infty$ (the coefficients $C_1, C_2, \dots$ do not depend on the conjugate variable). The singular dependence on L (more precisely, on the logarithm $\tilde{L}$ of the conjugate variable) is entirely *exponentiated* in the factor S:

$$S = \exp\left\{ L \, g_1(\alpha_{\rm S} L) + g_2(\alpha_{\rm S} L) + \alpha_{\rm S} \, g_3(\alpha_{\rm S} L) + \dots \right\} \quad . \tag{15}$$

In the exponent, the function $L \, g_1$ resums all the leading logarithmic (LL) contributions $\alpha_{\rm S}^n L^{n+1}$, while g_2 contains the next-to-leading logarithmic (NLL) terms $\alpha_{\rm S}^n L^n$ and so forth[§]

[§]To compare this notation with that of Ref. [68], we can notice that our functions g_i are obtained by the straightforward integration over $\overline{\mu}$ of the functions $A(\alpha_{\rm S}(\overline{\mu}))$ and $B(\alpha_{\rm S}(\overline{\mu}))$ of Ref. [68]. In particular, our terms g_1, g_2, g_3 are not to be confused with the non-perturbative parameters of the same name used in Ref. [68].

(all the functions g_i are normalized as $g_i(\lambda = 0) = 0$). Note that the LL terms are formally suppressed by a power of α_S with respect to the NLL terms, and so forth for the successive classes of logarithmic terms. Thus, this logarithmic expansion is as systematic as the fixed-order expansion in Eq. (9). In particular, using a matched NLL+NLO calculation, we can consistently *i*) introduce a precise definition (say $\overline{\rm MS}$) of $\alpha_S(\mu)$ and *ii*) investigate the theoretical accuracy of the calculation by studying its renormalization-scale dependence.

The structure of the exponentiated resummed calculations discussed so far has to be contrasted with that obtained by organizing the logarithmic expansion on the right-hand side of Eq. (10) in terms of towers as

$$\hat{\sigma} \sim \alpha_S^k \hat{\sigma}^{(LO)} \left\{ t_1(\alpha_S L^2) + \alpha_S L \; t_2(\alpha_S L^2) + \alpha_S^2 L^2 \; t_3(\alpha_S L^2) + \ldots \right\} \quad , \tag{16}$$

where the double-logarithmic function $t_1(\alpha_S L^2)$ and the successive functions are normalized as $t_i(0) = \text{const}$. While the ratio of two successive terms in the exponent of Eq. (15) is formally of the order of α_S, the ratio of two successive towers in Eq. (16) is formally of the order of $\alpha_S L$. In other words, the tower expansion sums the double-logarithmic terms $(\alpha_S L^2)^n$, then the terms $\alpha_S^n L^{2n-1} \sim \alpha_S L (\alpha_S L^2)^{n-1}$, and so forth; it thus assumes that the resummation procedure is carried out with respect to the large parameter $\alpha_S L^2$ ($\alpha_S L^2 \lesssim 1$). On the contrary, in Eq. (15) the large parameter is $\alpha_S L \lesssim 1$. The tower expansion allows us to formally extend the applicability of perturbative QCD to the region $L \lesssim 1/\sqrt{\alpha_S}$, and exponentiation extends it to the wider region $L \lesssim 1/\alpha_S$. This fact can also be argued by comparing the amount of information on the logarithmic terms that is included in the truncation of Eqs. (15) and (16) at some logarithmic accuracy. The reader can easily check that, after matching to the NLO (LO) calculation as in Eq. (11), the NLL (LL) result of Eq. (15) contains all the logarithms of the first *four* (*two*) towers in Eq. (16) (and many more logarithmic terms).

In the case of $Q_\perp$-distributions, full NLL resummation has been performed for lepton pairs, W and Z bosons produced by the DY mechanism [61, 66] and for Higgs bosons produced by gluon fusion [67]. Corresponding resummed calculations are discussed in Refs. [52, 68] and references therein.

Threshold logarithms in hadron collisions have been resummed to NLL accuracy for DIS and DY production [62, 63, 43, 69] and for Higgs boson production [70]. Recent theoretical progress [71, 72, 19] regards the extension of NLL resummation to processes produced by LO hard-scattering of more than two coloured partons, such as heavy-quark hadroproduction [71, 19] and leptoproduction [73], as well as prompt-photon [74–77], quarkonium [78] and vector-boson [79] production.

An important feature of threshold resummation is that the resummed soft-gluon contributions regard the partonic cross section rather than the hadronic cross section. This fact has two main consequences: *i*) soft-gluon contributions can be sizeable long before the threshold region in the hadronic cross section is actually approached, and *ii*) the resummation effects typically enhance the fixed-order perturbative calculations.

The first consequence follows from the fact that the evolution of the parton densities sizeably reduces the energy that is available in the partonic hard-scattering subprocess. Thus, the partonic cross section $\hat{\sigma}$ in the factorization formula (2) is typically evaluated

much closer to threshold than the hadronic cross section. In other words, the parton densities are strongly suppressed at large x (typically, when $x \to 1$, $f(x,\mu^2) \sim (1-x)^\eta$ with $\eta \sim 3$ and $\eta \sim 6$ for valence quarks and sea-quarks or gluons, respectively); after integration over them, the dominant value of the square of the partonic centre-of-mass energy $\langle \hat{s} \rangle = \langle x_1 x_2 \rangle S$ is therefore substantially smaller than the corresponding hadronic value S.

The second consequence, which depends on the actual definition of the parton densities, follows from the fact that the resummed contributions are those soft-gluon effects that are left at the partonic level after factorization of the parton densities. After having absorbed part of the full soft-gluon contributions in the customary definitions (for instance, those in the $\overline{\rm MS}$ or DIS factorization schemes) of the parton densities, it turns out that the residual effect in the partonic cross section is positive and tends to enhance the perturbative predictions.

A quantitative illustration of these consequences is given below by discussing top-quark and prompt-photon production. The discussion also shows another relevant feature of NLO+NLL calculations, namely, their increased stability with respect to scale variations.

The effects of soft-gluon resummation on the top-quark production cross sections at hadron colliders have been studied in Refs. [19, 80–83]. In the case of $p\bar{p}$ collisions, the comparison between QCD predictions at NLO and those after NLL resummation is shown in Fig. 10 [19]. At the Tevatron the resummation effects are not very large and the NLO cross section is increased by about 4%. This had to be expected because the top quark is not produced very close to threshold ($x = 2m_t/\sqrt{S} \sim 0.2$, at the Tevatron). Note, however, that the dependence on the factorization/renormalization scale of the theoretical cross section is reduced by a factor of almost 2 by including NLL resummation. More precisely, the scale dependence ($\sim \pm 5\%$) of the NLO+NLL calculation becomes comparable to that obtained by using different sets of parton densities [11]. Combining linearly scale and parton density uncertainties, the NLO+NLL cross section is $\sigma_{t\bar{t}} = 5.0 \pm 0.6$, with $m_t = 175$ GeV and $\sqrt{S} = 1.8$ TeV [19].

At the LHC ($x = 2m_t/\sqrt{S} \sim 0.03$) the top quark is produced less close to the hadronic threshold than at the Tevatron. However this is compensated by the fact that the gluon channel[¶] is more important at the LHC. As a result, the effect of including soft-gluon resummation to NLL accuracy is very similar: the NLO cross section is enhanced by $\sim 5\%$ and its scale dependence is reduced from $\sim \pm 10\%$ to $\sim \pm 5\%$. Note, however, that the uncertainty ($\sim \pm 10\%$) coming from the parton (gluon) densities is larger than at the Tevatron [7].

Similar qualitative results are obtained [76] when NLL resummation is applied to prompt-photon production at fixed-target experiments. The scale dependence of the theoretical calculation is highly reduced and the resummed NLL contributions lead to large corrections at high $x_T = 2E_T/\sqrt{S}$ (and smaller corrections at lower x_T). Of course, the impact of soft-gluon resummation is quantitatively more sizeable in prompt-photon pro-

[¶]Since f_g is steeper than f_q at large x, partonic cross sections in gluon subprocesses are typically closer to threshold than in quark subprocesses. Moreover, the intensity of soft-gluon radiation from gluons is larger than that from quarks by a factor of $\sim C_A/C_F \sim 2$.

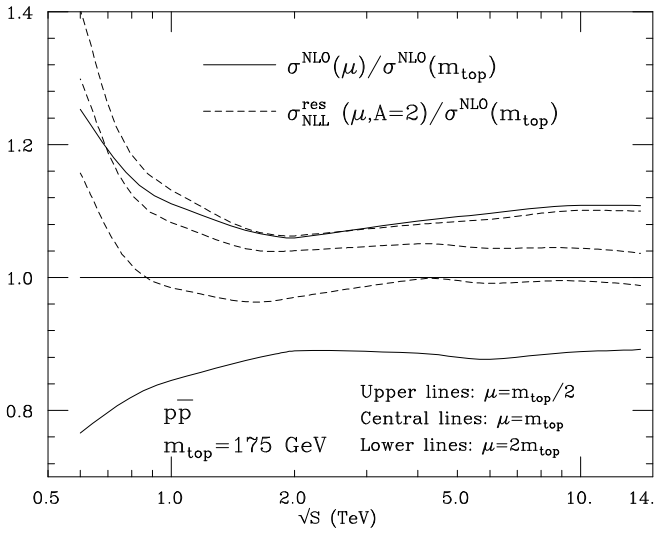

Figure 10: The $t\bar{t}$ production cross section in $p\bar{p}$ collisions as a function of $\sqrt{S}$. The solid lines represent the NLO results for different choices ($\mu = m_t/2$ and $\mu = 2m_t$) of the renormalization/factorization scale $\mu = \mu_R = \mu_F$, normalized to the result with $\mu = m_t$. The dashed lines represent the NLO+NLL results for different choices of μ ($\mu = m_t/2, m_t$ and $2m_t$), normalized to the NLO result with $\mu = m_t$.

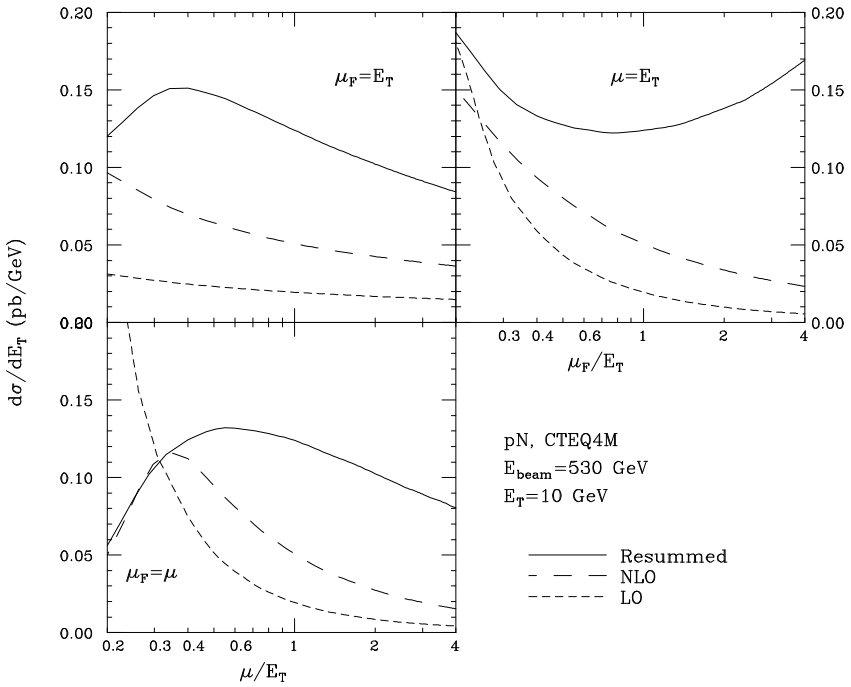

Figure 11: The dependence on the factorization (μ_F) and renormalization ($\mu_R = \mu$) scale of the prompt-photon cross section $d\sigma/dE_T$ in pN collisions at $E_T = 10$ GeV and $\sqrt{S} = 31.6$ GeV. The short-dashed, long-dashed and solid lines are respectively the results at LO, NLO and after NLO+NLL resummation.

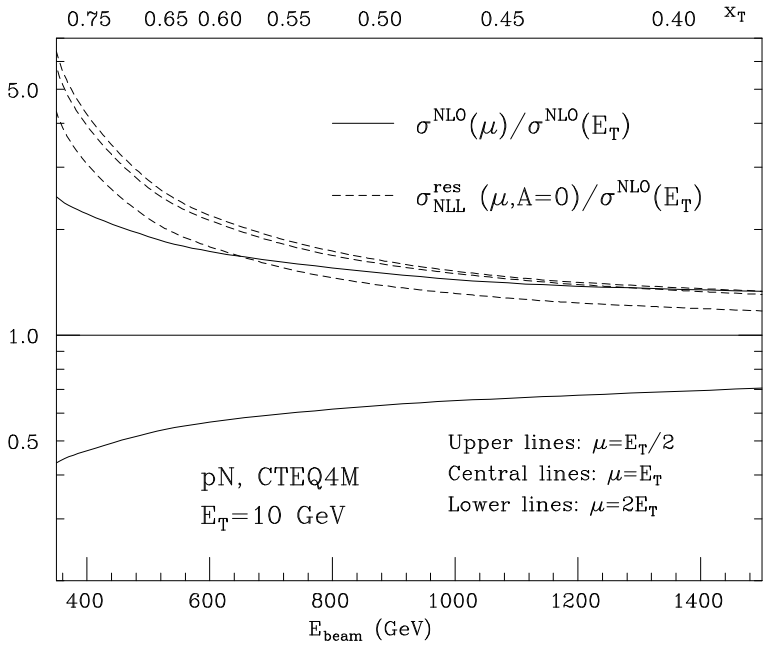

Figure 12: The prompt-photon cross section $d\sigma/dE_T$ in pN collisions at $E_T = 10$ GeV as a function of the energy $E_{\rm beam}$ of the proton beam. The solid lines represent the NLO results for different choices ($\mu = E_T/2$ and $\mu = 2E_T$) of the renormalization/factorization scale $\mu = \mu_R = \mu_F$, normalized to the result with $\mu = E_T$. The dashed lines represent the NLO+NLL results for different choices of μ ($\mu = E_T/2, E_T$ and $2E_T$), normalized to the NLO result with $\mu = E_T$.

duction than in top-quark production, because x_T can be as large as 0.6, the hard scale E_T is much smaller than m_t (thus, $\alpha_{\rm S}(E_T) > \alpha_{\rm S}(m_t)$) and the gluon channel is always important. The scale dependence of the theoretical cross section for the E706 kinematics is shown in Fig. 11. Fixing $\mu_R = \mu_F = \mu$ and varying μ in the range $E_T/2 < \mu < 2E_T$ with $E_T = 10$ GeV, the cross section varies by a factor of ~ 6 at LO, by a factor of ~ 4 at NLO and by a factor of ~ 1.3 after NLL resummation. The highly reduced scale dependence of the NLO+NLL cross section is also visible in Fig. 12, which, in particular, shows that when $E_T = 10$ GeV and $E_{\rm beam} = 530$ GeV the central value (i.e. with $\mu = E_T$) of the NLO cross section increases by a factor of ~ 2.5 after NLL resummation. As expected, the size of these effects is reduced by increasing $\sqrt{S}$ at fixed E_T (see Fig. 12) or by decreasing E_T at fixed $\sqrt{S}$ (see Fig. 8).

The comparison with the E706 data shown in Fig. 13 suggests that the NLO+NLL calculation can help to better understand prompt-photon production at large x_T. Note, however, that this comparison has to be regarded as preliminary in several respects [76]. In particular, the parton densities used in Fig. 13 are those extracted from NLO fits. Owing to the soft-gluon enhancement at large x_T, refitting the parton densities may lead to a smaller f_g at large x and, consequently (because of the momentum sum rule), a larger f_g at intermediate x. As a result, this procedure could somehow increase the theoretical cross section also at smaller values of x_T.

Soft-gluon resummation at NLL accuracy is now available for all the processes (namely, DIS, DY and prompt-photon production) that are typically used to perform global fits to

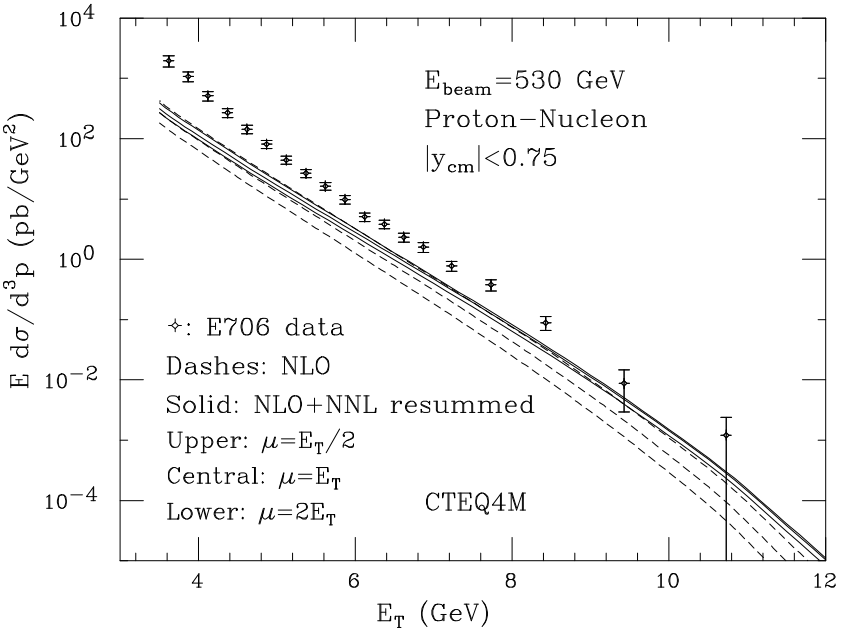

Figure 13: E706 prompt-photon data compared with theoretical calculations, which use the parton densities of the set CTEQ4 and GRV photon fragmentation functions. The solid and dashed lines correspond to the NLO+NLL and pure NLO calculations, respectively.

parton densities. A detailed extraction/evolution of parton densities by consistently using NLL resummed calculations is thus nowadays feasible.

6 Other topics

The activity of the QCD Working Group at this Workshop has also been devoted to other topics, such as automatic computation of matrix elements and LO cross sections for multiparticle processes at high-energy colliders, definition and properties of jets algorithms, definition of isolated photons and related NLO calculations. Corresponding contributions are included in these Proceedings.

Other studies performed during this Workshop have a large overlap with the activity of the related Workshops at FERMILAB and CERN and can be found in those Proceedings [6, 7].

Acknowledgements. I would like to thank the members of the Local Organizing Committee for the excellent Workshop.

References

1. M.L. Mangano, plenary talk at the *1999 International Europhysics Conference on High Energy Physics* Tampere, Finland, 15–21 July 1999, preprint CERN-TH/99-337

(hep-ph/9911256), to appear in the Proceedings, and references therein.

2. B.R. Webber, plenary talk at the *19th International Symposium on Lepton-Photon Interactions at High-Energies, LP 99*, Stanford, California, 9–14 Aug 1999, preprint CERN-TH/99-387 (hep-ph/9912292), to appear in the Proceedings, and references therein.

3. J. Huston, in Proc. of the *29th International Conference on High-Energy Physics, ICHEP 98*, eds. A. Astbury, D. Axen and J. Robinson (World Scientific, Singapore, 1999), vol. 1, p. 283, and references therein.

4. S. Catani, hep-ph/9712442, in Proc. of the *XVIII International Symposium on Lepton-Photon Interactions, LP97*, eds. A. De Roeck and A. Wagner (World Scientific, Singapore, 1998), p. 147, and references therein.

5. G. Jarlskog and D. Rein eds., Proc. of ECFA LHC Workshop, report CERN 90-10 (December 1990); ATLAS Coll., ATLAS TDR 15, report CERN/LHCC/99-15 (May 1999).

6. Proceedings of the Workshop on *Physics at the Tevatron in Run II*, Fermilab, 2000 (to appear). See: http://www-theory.fnal.gov/people/ellis/QCDWB/QCDWB.html

7. Proceedings of the Workshop on *Standard Model Physics (and more) at the LHC*, CERN 1999 (to appear). See: http://home.cern.ch/˜mlm/lhc99/lhcworkshop.html

8. See J.C. Collins, D.E. Soper and G. Sterman, in *Perturbative Quantum Chromodynamics*, ed. A.H. Mueller (World Scientific, Singapore, 1989), p. 1, and references therein.

9. V.N. Gribov and L.N. Lipatov, Sov. J. Nucl. Phys. 15 (1972) 438, 675; G. Altarelli and G. Parisi, Nucl. Phys. B126 (1977) 298; Yu.L. Dokshitzer, Sov. Phys. JETP 46 (1977) 641.

10. E. G. Floratos, D. A. Ross and C. T. Sachrajda, Nucl. Phys. B129 (1977) 66, E ibid. B139 (1978) 545, Nucl. Phys. B152 (1979) 493; A. Gonzalez-Arroyo, C. Lopez and F. J. Yndurain, Nucl. Phys. B153 (1979) 161; A. Gonzalez-Arroyo and C. Lopez, Nucl. Phys. B166 (1980) 429; G. Curci, W. Furmanski and R. Petronzio, Nucl. Phys. B175 (1980) 27; W. Furmanski and R. Petronzio, Phys. Lett. B97 (1980) 437; E. G. Floratos, C. Kounnas and R. Lacaze, Nucl. Phys. B192 (1981) 417.

11. A.D. Martin, R.G. Roberts, W.J. Stirling and R.S. Thorne, Eur. Phys. J. C4 (1998) 463, Phys. Lett. 443B (1998) 301, preprint DTP-99-64 (hep-ph/9907231); M. Glück, E. Reya and A. Vogt, Eur. Phys. J. C5 (1998) 461; H.L. Lai et al., Eur. Phys. J. C12 (2000) 375.

12. LHC Guide to Parton Distribution Functions and Cross Sections, ATLAS note ATL-PHYS-99-008, http://www.pa.msu.edu/˜huston/lhc/lhc_pdfnote.ps .

13. R.D. Ball, in these Proceedings, and references therein.

14. U.K. Yang and A. Bodek, Phys. Rev. Lett. 82 (1999) 2467, preprint UR-1581 (hep-ex/9908058).

15. W. Melnitchouk, I.R. Afnan, F. Bissey and A.W. Thomas, preprint ADP-99-47-T384 (hep-ex/9912001).

16. S. Kuhlmann et al., hep-ph/9912283.

17. J. Huston et al., Phys. Rev. D 58 (1998) 114034.

18. R. Hamberg, W.L. van Neerven and T. Matsuura, Nucl. Phys. B359 (1991) 343; W.L. van Neerven and E.B. Zijlstra, Nucl. Phys. B382 (1992) 11.

19. R. Bonciani, S. Catani, M.L. Mangano and P. Nason, Nucl. Phys. B529 (1998) 424.

20. L.N. Lipatov, Sov. J. Nucl. Phys. 23 (1976) 338; E.A. Kuraev, L.N. Lipatov and V.S. Fadin, Sov. Phys. JETP 45 (1977) 199; Ya. Balitskii and L.N. Lipatov, Sov. J. Nucl. Phys. 28 (1978) 822.

21. T. Jaroszewicz, Phys. Lett. 116B (1982) 291.

22. S. Catani and F. Hautmann, Phys. Lett. 315B (1993) 157, Nucl. Phys. B427 (1994) 475.

23. V.S. Fadin and L.N. Lipatov, Sov. J. Nucl. Phys. 50 (1989) 712, Phys. Lett. 429B (1998) 127.

24. M. Ciafaloni and G. Camici, Nucl. Phys. B496 (1997) 305, Phys. Lett. 430B (1998) 349.

25. S. Catani, Z. Phys. C70 (1996) 263, Z. Phys. C75 (1997) 665.

26. P. Nason, S. Dawson and R.K. Ellis, Nucl. Phys. B303 (1988) 607; W. Beenakker, H. Kuijf, W.L. van Neerven and J. Smith, Phys. Rev. D 40 (1989) 54; M.L. Mangano, P. Nason and G. Ridolfi, Nucl. Phys. B373 (1992) 295.

27. M. Baarmand, talk presented at the Workshop on *Standard Model Physics (and more) at the LHC*, CERN, January 1999.
See: http://home.cern.ch/n/nason/www/lhc99/14-01-99/program-1-14-99

28. S. Frixione, M.L. Mangano, P. Nason and G. Ridolfi, in *Heavy Flavours II*, eds. A.J. Buras and M. Lindner (World Scientific, Singapore, 1998), p. 609, and references therein.

29. M. Cacciari, M. Greco and P. Nason, JHEP 05 (1998) 007; F.I. Olness, R.J. Scalise and Wu-Ki Tung, Phys. Rev. D 59 (1999) 014506.

30. S. Catani, M. Ciafaloni and F. Hautmann, Phys. Lett. 242B (1990) 97, Nucl. Phys. B366 (1991) 135; J.C. Collins and R.K. Ellis, Nucl. Phys. B360 (1991) 3; E.M. Levin, M.G. Ryskin, Yu.M. Shabel'skii and A.G. Shuvaev, Sov. J. Nucl. Phys. 53 (1991) 657.

31. P. Aurenche, R. Baier, M. Fontannaz and D. Schiff, Nucl. Phys. B297 (1988) 661; H. Baer, J. Ohnemus and J.F. Owens, Phys. Rev. D 42 (1990) 61; P. Aurenche, R. Baier and M. Fontannaz, Phys. Rev. D 42 (1990) 1440; L.E. Gordon and W. Vogelsang, Phys. Rev. D 48 (1993) 3136.

32. P. Aurenche, M. Fontannaz, J.Ph. Guillet, B. Kniehl, E. Pilon and M. Werlen, Eur. Phys. J. C9 (1999) 107.

33. E706 Coll., L. Apanasevich et al., Phys. Rev. Lett. 81 (1998) 2642.

34. L. Apanasevich et al., Phys. Rev. D 59 (1999) 074007.

35. M.A. Kimber, A.D. Martin and M.G. Ryskin, Eur. Phys. J. C12 (2000) 655.

36. E. Laenen, G. Sterman and W. Vogelsang, preprint YITP-99-69 (hep-ph/0002078).

37. P. Aurenche, M. Fontannaz, J.P. Guillet, B.A. Kniehl and M. Werlen, preprint LAPTH-751-99 (hep-ph/9910252).

38. J. Huston et al., paper in preparation.

39. V. Del Duca and G. Heinrich, in these Proceedings, and references therein.

40. R.K. Ellis, W.J. Stirling and B.R. Webber, *QCD and Collider Physics* (Cambridge University Press, Cambridge, 1996) and references therein.

41. Yu.L. Dokshitzer, V.A. Khoze, A.H. Mueller and S.I. Troian, *Basics of Perturbative QCD* (Editions Frontières, Gif-sur-Yvette, 1991) and references therein.

42. A. Bassetto, M. Ciafaloni and G. Marchesini, Phys. Rep. 100 (1983) 201, and references therein.

43. S. Catani, G. Marchesini and B.R. Webber, Nucl. Phys. B349 (1991) 635.

44. M.H. Seymour, Comput. Phys. Commun. 90 (1995) 95.

45. J. Andre and T. Sjostrand, Phys. Rev. D57 (1998) 5767.

46. C. Friberg and T. Sjostrand, in Proc. of the Workshop *Monte Carlo Generators for HERA Physics*, eds. T.A. Doyle, G. Grindhammer, G. Ingelman and H. Jung, (DESY, Hamburg, 1999), p. 181.

47. J.C. Collins, hep-ph/0001040 and in these Proceedings.

48. G. Corcella and M.H. Seymour, Phys. Lett. 442B (1998) 417.

49. G. Miu and T. Sjostrand, Phys. Lett. 449B (1999) 313.

50. S. Mrenna, preprint UCD-99-4 (hep-ph/9902471).

51. G. Corcella and M.H. Seymour, preprint RAL-TR-1999-051 (hep-ph/9908388).

52. C. Balazs, J. Huston and I. Puljak, preprint FERMILAB-PUB-00-032-T (hep-ph/0002032), and in these Proceedings.

53. G. Sterman, in Proc. *10th Topical Workshop on Proton-Antiproton Collider Physics*, eds. R. Raja and J. Yoh (AIP Press, New York, 1996), p. 608; S. Catani, Nucl. Phys. Proc. Suppl. 54A (1997) 107, and in Proc of the *32nd Rencontres de Moriond: QCD and High-Energy Hadronic Interactions*, ed. J. Tran Than Van (Editions Frontières, Paris, 1997), p. 331.

54. S. Catani, G. Turnock, B.R. Webber and L. Trentadue, Nucl. Phys. B407 (1993) 3.

55. M.H. Seymour, Nucl. Phys. B513 (1998) 269; J.R. Forshaw and M.H. Seymour, JHEP 09 (1999) 009.

56. Yu.L. Dokshitzer, D.I. Diakonov and S.I. Troian, Phys. Rep. 58 (1980) 269, and references therein.

57. N. Brown and W.J. Stirling, Phys. Lett. 252B (1990) 657.

58. S. Catani, Yu.L. Dokshitzer, M. Olsson, G. Turnock and B.R. Webber, Phys. Lett. 269B (1991) 432.

59. S. Catani, Yu.L. Dokshitzer and B.R. Webber, Phys. Lett. 285B (1992) 291; S. Catani, Yu.L. Dokshitzer, M.H. Seymour and B.R. Webber, Nucl. Phys. B406 (1993) 187; S.D. Ellis and D.E. Soper, Phys. Rev. D 48 (1993) 3160.

60. G. Parisi and R. Petronzio, Nucl. Phys. B154 (1979) 427.

61. J.C. Collins, D.E. Soper and G. Sterman, Nucl. Phys. B250 (1985) 199.

62. G. Sterman, Nucl. Phys. B281 (1987) 310.

63. S. Catani and L. Trentadue, Nucl. Phys. B327 (1989) 323, Nucl. Phys. B353 (1991) 183.

64. J.C. Collins and D.E. Soper, Nucl. Phys. B197 (1982) 446.

65. S. Catani, M.L. Mangano, P. Nason and L. Trentadue, Nucl. Phys. B478 (1996) 273.

66. J. Kodaira and L. Trentadue, Phys. Lett. 112B (1982) 66, Phys. Lett. 123B (1983) 335; C.T.H. Davies, B.R. Webber and W.J. Stirling, Nucl. Phys. B256 (1985) 413.

67. S. Catani, E. D'Emilio and L. Trentadue, Phys. Lett. 211B (1988) 335; R.P. Kauffman, Phys. Rev. D 45 (1992) 1512.

68. C. Balázs, J.C. Collins and D.E. Soper, in these Proceedings.

69. H. Contopanagos, E. Laenen and G. Sterman, Nucl. Phys. B484 (1997) 303.

70. M. Kramer, E. Laenen and M. Spira, Nucl. Phys. B511 (1998) 523.

71. N. Kidonakis and G. Sterman, Phys. Lett. 387B (1996) 867, Nucl. Phys. B505 (1997) 321.

72. N. Kidonakis, G. Oderda and G. Sterman, Nucl. Phys. B531 (1998) 365.

73. E. Laenen and S. Moch, Phys. Rev. D 59 (1999) 034027.

74. E. Laenen, G. Oderda and G. Sterman, Phys. Lett. 438B (1998) 173.

75. S. Catani, M.L. Mangano and P. Nason, JHEP 07 (1998) 024.

76. S. Catani, M.L. Mangano, P. Nason, C. Oleari and W. Vogelsang, JHEP 03 (1999) 025.

77. N. Kidonakis and J.F. Owens, preprint FSU-HEP-991216 (hep-ph/9912388).

78. M. Cacciari, preprint CERN-TH/99-312 (hep-ph/9910412).

79. N. Kidonakis and V. Del Duca, preprint FSU-HEP-991123 (hep-ph/9911460).

80. E. Laenen, J. Smith and W.L. van Neerven, Nucl. Phys. B369 (1992) 543, Phys. Lett. 321B (1994) 254.

81. E. Berger and H. Contopanagos, Phys. Rev. D 54 (1996) 3085, Phys. Rev. D 57 (1998) 253.

82. S. Catani, M.L. Mangano, P. Nason and L. Trentadue, Phys. Lett. 378B (1996) 329.

83. N. Kidonakis, preprint EDINBURGH-99-4 (hep-ph/9904507).